

A vector total variation of feature image model for image restoration

Wei Wang*, Xiang-Gen Xia^{*†}, Shengli Zhang*, Chuanjiang He[‡]

February 13, 2018

Abstract

In this paper, we propose a vector total variation (VTV) of feature image model for image restoration. The VTV imposes different smoothing powers on different features (e.g. edges and cartoons) based on choosing various regularization parameters. Thus, the model can simultaneously preserve edges and remove noises. Next, the existence of solution for the model is proved and the split Bregman algorithm is used to solve the model. At last, we use the wavelet filter banks to explicitly define the feature operator and present some experimental results to show its advantage over the related methods in both quality and efficiency.

keywords. Image restoration, wavelet, vectore total variation, variational method

1 Introduction

Image restoration including image denoising, deblurring, inpainting etc. is a procedure of improving the quality of a given image that is degraded in various ways during the process of acquisition and commutation. Since many advanced applications in computer vision depend heavily on the input of high quality images, image restoration becomes an indispensable and preprocessing step of these applications. Therefore, image restoration is a basic but very important area in image processing and analysis. Image restoration can be modeled as a linear inverse problem:

$$f = Au + \eta$$

*College of Information Engineering, Shenzhen University, Shenzhen, China. (aiyulunhui@sina.com, xxia@ee.udel.edu, zsl@szu.edu.cn cjhe@cqu.edu.cn)

[†]Department of Electrical and Computer Engineering, University of Delaware, Newark, DE 19716, USA.

[‡]College of Mathematics and Statistics, Chongqing University, Chongqing 401331, China.

This research is partially supported by the research grants from the Chinese NSF project (61372078), National Natural Science Foundation of China (No. 61701320, No. 61561019), Guangdong NSF project (2014A030313549), Key project of Guangdong (2016KZDXM006) and the Shenzhen NSF project (JCYJ20160226192223251).

where f is the observed images, A is a linear operator and η represents the additive noise whose type depends on its probability density function (PDF). The goal of image restoration is to find the unknown true image u from the observed image f . The problem is usually an ill-posed inverse problem and often solved by imposing a prior regularization assumption. Among all regularization-based methods for image restoration, variational based [1][2][3][4][5][6][7] and wavelet frame based [8][9][10][11][12][13][14][15][12][13][14][15][16][17][18] methods have attracted a lot of attention in the past.

The common assumption of the regularization based methods is that images can be sparsely approximated in some transformed domains. Such transforms can be gradient operator, wavelet frame transform, Fourier transform, Gabor transform etc. In order to utilize the sparsity, one solves (1) by finding a sparse solution in the corresponding transformed domain. Typically, the l_1 norm is used as a penalty of the sparsity. One of the well-known variational approaches is the Rudin-Osher-Fatemi (ROF) [19] model, which imposes the total variation (TV) regularization on the image u :

$$\inf_{u \in BV(\Omega)} \left\{ \lambda \int_{\Omega} |\nabla u| + \int_{\Omega} (u - f)^2 dx \right\}.$$

Here, Ω is the image domain, $BV(\Omega)$ is the bounded variational space, $\int_{\Omega} |\nabla u|$ and $\int_{\Omega} (u - f)^2 dx$ are the TV (regularization) term and fidelity (fitting) term, respectively. The ROF model performs well for removing noise while preserving edges. However, it tends to produce piecewise constant results (called staircase effect in the literature). After the ROF model was proposed, the TV regularization has been extended to many other image restoration applications (such as deblurring, inpainting, superresolution, etc.) and has been modified in a variety of ways to improve its performance [20][21][22][23]. To solve the ROF model, many algorithms have been proposed [24][25][26][27][28] [29][30] and the split Bregman method [28] is the one of the most widely used ones.

Wavelet frames represent images as a summarization of smooth components (i.e. cartoon), and local features (i.e. singularities). In wavelet frame domain, smooth image components are the coefficient images obtained from low-pass filters, while local features are those obtained from high-pass filters. Thus, we can impose different strengths of regularization on smooth components and local features separately when restoring images in the wavelet frame transform domain. There exist plenty of wavelet frame based image restoration models in the literature, such as, the synthesis based approach [8][9][10][11], the analysis based approach [12][13][14][15], and the balanced approach [16][17][18]. A typical analysis based model of l_1 norm regularization has a similar form with the ROF model:

$$\min_u \lambda \|Wu\|_1 + \frac{1}{2} \|Au - f\|_2^2,$$

where W represents the wavelet frame transform. Since the l_1 norm regularizations usually exist in the wavelet frame based models, the split Bregman algorithm is also a widely used method to solve them.

In this paper, we propose a vector total variation (VTV) of feature image model for image restoration where the VTV is used as the regularization. The vector images are generated by mapping the original image into the feature spaces which represent different features of the image such as edges and cartoons. By choosing different regularization parameters, we can impose different smoothing powers on different features. Thus, the model can simultaneously preserve edges and remove noises. Next, the existence of solution for the model is proved and the split Bregman algorithm is used to solve the model. At last, we use the wavelet filter banks to explicitly define the feature operator and present some experimental results to show its advantage over the related methods in both quality and efficiency.

The rest of the paper is organized as follows. In Section 2.1, we describe the proposed model, prove the existence of its solution and use the convolution to define the feature operators. In Section 2.2, we use the split Bregman algorithm to solve the model. In Section 3, we present some experimental results to show the advantage of our model. In Section 4, we conclude this paper.

2 The wavelet coefficient total variational model

2.1 Proposed model

Before describing the model, we briefly introduce some mathematical definitions related to our paper.

Let Ω be a bounded open subset of R^2 , $f \in L^2(\Omega, R)$, $F = (F_1, F_2, \dots, F_m)$ be an operator such that $Ff = (F_1f, F_2f, \dots, F_mf) \in L^2(\Omega, R^m)$ and $F_i f \in L^2(\Omega, R)$. In this paper, we call $F_i f$ a feature image of f and F a feature operator.

Definition 1. The inner product in $L^2(\Omega, R^m)$ is defined as

$$\langle u, v \rangle_{L^2(\Omega, R^m)} = \int_{\Omega} \sum_{i=1}^m u_i v_i,$$

where $u = (u_1, u_2, \dots, u_m)$, $v = (v_1, v_2, \dots, v_m) \in L^1(\Omega, R^m)$.

Definition 2. $BV(\Omega)$ is the subspace of $L^1(\Omega, R)$ such that the following quantity is finite:

$$|f|_{TV} = \sup_{\eta \in K} \langle f, \operatorname{div} \eta \rangle_{L^2(\Omega, R)},$$

where $\operatorname{div} \eta = \frac{\partial \eta_1}{\partial x} + \frac{\partial \eta_2}{\partial y}$, $K = \{\eta = (\eta_1, \eta_2) \in C_0^1(\Omega, R^2) : \|\eta\|_{L^\infty(\Omega, R^2)} \leq 1\}$, $C_0^1(\Omega, R^2)$ is the space of continuously differentiable functions with compact support in Ω , $\|\eta\|_{L^\infty(\Omega, R^2)} = \sup_{x \in \Omega} \sqrt{\eta_1^2 + \eta_2^2}$ and the quantity $|f|_{TV}$ is called the total variation of f .

Definition 3. The vector total variation of function $g = (g_1, g_2, \dots, g_m) \in L^1(\Omega, R^m)$ is defined as

$$|g|_{VTV} = \sup_{\xi \in P} \langle g, \operatorname{div} \xi \rangle_{L^2(\Omega, R^m)},$$

where $\xi = (\xi_1, \xi_2, \dots, \xi_m)$, $\operatorname{div} \xi = (\operatorname{div} \xi_1, \operatorname{div} \xi_2, \dots, \operatorname{div} \xi_m)$, $P = \{\xi \in C_0^1(\Omega, R^{2 \times m}) : \|\xi(x)\|_{L^\infty(\Omega, R^{2 \times m})} \leq 1\}$ and $\|\xi(x)\|_{L^\infty(\Omega, R^{2 \times m})} = \max_{i=1,2,\dots,m} \|\xi_i(x)\|_{L^\infty(\Omega, R^2)}$.

For g smooth enough, we have [31][32]

$$|g|_{VTV} = \sum_{i=1}^m |g_i|_{TV} = \sum_{i=1}^m \int_{\Omega} |\nabla g_i|. \quad (1)$$

For more details about the vector total variation, refer to [31][32][33][34][35].

In this paper, we propose the following model for image recovery:

$$\arg \inf_{u \in BV(\Omega)} \{E(u) = |\vec{\lambda} F u|_{VTV} + \frac{1}{2} \|Au - f\|_{L^2(\Omega, R)}^2\}, \quad (2)$$

where A is a linear operator, f is an observed image, F is a feature operator, $\vec{\lambda} = (\lambda_1, \lambda_2, \dots, \lambda_m) \in (R^+)^m$ is the regularization parameter vector and $\vec{\lambda} F u = (\lambda_1 F_1 u, \lambda_2 F_2 u, \dots, \lambda_m F_m u)$ represents the feature images. The ideal case is that different $F_m u$ can represent different features of the image u , such as edges, cartoons, etc. and thus we can impose different smooth strengths on them by choosing different λ_i . Clearly, if $m = 1$ and $F = I$, then the proposed model is reduced to the ROF model.

In the following, we show the existence of the solution for problem (2).

Lemma 1. If F_i is linear, then the adjoint operator F^* of F is

$$F^* g = \sum_{i=1}^m F_i^* g_i,$$

where $g = (g_1, g_2, \dots, g_m) \in L^2(\Omega, R^m)$ and F_i^* is the adjoint operator of F_i .

Proof. Let $f \in L^2(\Omega, R)$ and $g \in L^2(\Omega, R^m)$, then

$$\begin{aligned} \langle F f, g \rangle &= \sum_{i=1}^m \langle F_i f, g_i \rangle \\ &= \sum_{i=1}^m \langle f, F_i^* g_i \rangle \\ &= \langle f, \sum_{i=1}^m F_i^* g_i \rangle \end{aligned}$$

Thus, $F^* g = \sum_{i=1}^m F_i^* g_i$. □

Lemma 2. If F is linear and bounded and for any $\xi \in C_0^1(\Omega, R^{2 \times m})$, the operator div and F^* are commutative, i.e., $F^* \text{div} \xi = \text{div} F^* \xi$, then for any $f \in BV(\Omega)$, we have

$$|Ff|_{VTV} \leq \|F\| |f|_{TV}.$$

Proof.

$$\begin{aligned} |Ff|_{VTV} &= \sup_{\xi \in P} \langle Ff, \text{div} \xi \rangle \\ &= \sup_{\xi \in P} \langle f, F^* \text{div} \xi \rangle \\ &= \sup_{\xi \in P} \|F^* \xi\|_{L^\infty(\Omega, R^2)} \langle f, \text{div} \left(\frac{F^* \xi}{\|F^* \xi\|_{L^\infty(\Omega, R^2)}} \right) \rangle \\ &\leq \sup_{\xi \in P} \|F^*\| \|\xi\|_{L^\infty(\Omega, R^{2 \times m})} \langle f, \text{div} \left(\frac{F^* \xi}{\|F^* \xi\|_{L^\infty(\Omega, R^2)}} \right) \rangle \\ &\leq \|F^*\| |f|_{TV} \\ &= \|F\| |f|_{TV} \end{aligned}$$

□

Lemma 3. If F is linear and bounded, invertible, and for any $\eta \in C_0^1(\Omega, R^2)$, the operator div and $(F^{-1})^*$ are commutative, i.e., $(F^{-1})^* \text{div} \eta = \text{div} (F^{-1})^* \eta$, then for any $f \in BV(\Omega)$, we have

$$|f|_{TV} \leq \|F^{-1}\| |Ff|_{VTV}.$$

Proof.

$$\begin{aligned} |f|_{TV} &= \sup_{\eta \in K} \langle F^{-1} Ff, \text{div} \eta \rangle \\ &= \sup_{\eta \in K} \langle Ff, (F^{-1})^* \text{div} \eta \rangle \\ &= \sup_{\eta \in K} \|(F^{-1})^* \eta\|_{L^\infty(\Omega, R^{2 \times m})} \langle Ff, \text{div} \left(\frac{(F^{-1})^* \eta}{\|(F^{-1})^* \eta\|_{L^\infty(\Omega, R^{2 \times m})}} \right) \rangle \\ &\leq \sup_{\eta \in K} \|(F^{-1})^*\| \|\eta\|_{L^\infty(\Omega, R^2)} \langle Ff, \text{div} \left(\frac{(F^{-1})^* \eta}{\|(F^{-1})^* \eta\|_{L^\infty(\Omega, R^{2 \times m})}} \right) \rangle \\ &\leq \|(F^{-1})^*\| \sup_{\eta \in K} \langle Ff, \text{div} \left(\frac{(F^{-1})^* \eta}{\|(F^{-1})^* \eta\|_{L^\infty(\Omega, R^{2 \times m})}} \right) \rangle \\ &\leq \|(F^{-1})^*\| |Ff|_{VTV} \end{aligned}$$

□

Remark 1. From the proof, we can see the condition we need is that there exists $F_L^{-1} : L^2(\Omega, R^m) \rightarrow L^2(\Omega, R)$ such that $F_L^{-1} F = I$ and $(F_L^{-1})^* \text{div} \eta = \text{div} (F_L^{-1})^* \eta$ for any $\eta \in C_0^1(\Omega, R^2)$.

Lemma 4. If F is linear and bounded, and invertible, then for any $\xi \in C_0^1(\Omega, R^{2 \times m})$ and $\eta \in C_0^1(\Omega, R^2)$, the following two conditions are equivalent:

- (a) $F^* \operatorname{div} \xi = \operatorname{div} F^* \xi$,
- (b) $(F^{-1})^* \operatorname{div} \eta = \operatorname{div} (F^{-1})^* \eta$.

Proof. By (a) \Rightarrow (b) : Let $\xi = (F^{-1})^* \eta$ in (a), then

$$F^* \operatorname{div} (F^{-1})^* \eta = \operatorname{div} F^* (F^{-1})^* \eta = \operatorname{div} (F^{-1} F)^* \eta = \operatorname{div} \eta.$$

Multiplying $(F^{-1})^*$ on both sides of the above equation, we obtain

$$\operatorname{div} (F^{-1})^* \eta = (F^{-1})^* \operatorname{div} \eta,$$

(b) \Rightarrow (a) : Let $\eta = F^* \xi$ in (b), then we have

$$(F^{-1})^* \operatorname{div} F^* \xi = \operatorname{div} (F^{-1})^* F^* \xi = \operatorname{div} \xi.$$

Therefore,

$$\operatorname{div} F^* \xi = F^* \operatorname{div} \xi.$$

□

Remark 2. By $1 = \|F^{-1} F\| \leq \|F^{-1}\| \|F\|$, we only have $\|F^{-1}\| \geq \|F\|^{-1}$. If $\|F^{-1}\| = \|F\|^{-1}$, then combining Lemma 2 and Lemma 3, we can obtain $|Ff|_{VTV} = \|F\| |f|_{TV}$.

Theorem 1. If the conditions of Remark 1 are satisfied, $\lambda_{\min} = \min_{i=1,2,\dots,m} \lambda_i > 0$ and $A \otimes 1 = \int_{\Omega} A(x) dx \neq 0$, then Problem (2) admits a solution.

Proof. Let u_n be a minimizing sequence of Problem (2), then there exists a constant $M > 0$ such that $E(u_n) \leq M$, i.e.

$$\left| \vec{\lambda} F u \right|_{VTV} + \frac{1}{2} \|A u - f\|_{L^2(\Omega, R)}^2 \leq M.$$

Therefore,

$$\left| \vec{\lambda} F u \right|_{VTV} \leq M \tag{3}$$

$$\|A u - f\|_{L^2(\Omega, R)}^2 \leq 2M \tag{4}$$

From equation (3), by Lemma 3, we have

$$\begin{aligned} |u|_{TV} &\leq \|F^{-1}\| |F u|_{VTV} \\ &\leq \frac{1}{\lambda_{\min}} \|F^{-1}\| |\vec{\lambda} F u|_{VTV} \\ &\leq \frac{M}{\lambda_{\min}} \|F^{-1}\| \end{aligned} \tag{5}$$

As proved in in [33][36], from equation (4), we can obtain

$$\|u\|_{L^2(\Omega, R)} \leq M \quad (6)$$

Combining equations (5) and (6), we have that the sequence $\{u_n\}$ is bounded in $BV(\Omega)$. Thus, there exists $u^* \in BV(\Omega)$ such that u_n converges to u^* weakly in $L^2(\Omega)$ and strongly in $L^1(\Omega)$. Since the operator F is linear and bounded, we have that Fu_n also converges to Fu^* weakly in $L^2(\Omega)$ and strongly in $L^1(\Omega)$. Then a standard process can show that u^* is a minimizer of $E(u)$. \square

Theorem 2. If there exists a F_k such that F_k is invertible and $F_k \operatorname{div} \eta = \operatorname{div} F_k \eta$ for any $\eta \in C_0^1(\Omega, R^2)$, $\lambda_{\min} = \min_{i=1,2,\dots,m} \lambda_i > 0$ and $A \otimes 1 = \int_{\Omega} A(x) dx \neq 0$, then Problem (2) admits a solution.

Proof. Let u_n be a minimizing sequence of Problem (2), then there exists a constant $M > 0$ such that $E(u_n) \leq M$, i.e.

$$\left| \vec{\lambda} F u \right|_{VTV} + \frac{1}{2} \|Au - f\|_{L^2(\Omega, R)}^2 \leq M.$$

Therefore,

$$\left| \vec{\lambda} F u \right|_{VTV} = \sum_i^m |\lambda_i F_i u|_{TV} \leq M$$

and so

$$|F_k u|_{TV} \leq \frac{M}{\lambda_k}$$

Since F_k is invertible and $F_k \operatorname{div} \eta = \operatorname{div} F_k \eta$ for any $\eta \in C_0^1(\Omega, R^2)$, like the proof in Lemma 2, we can obtain

$$|u|_{TV} \leq \|F_k^{-1}\| |F_k u|_{TV} \leq \frac{M}{\lambda_k} \|F_k^{-1}\|$$

The left part of the proof is the same as that in Theorem 1 and so is omitted. \square

Remark 3. To assure the existence of the solution, we can intentionally design a F_k such that F_k satisfies the conditions in Theorem 2. The simplest F_k satisfying the conditions is $F_k = I$.

In the following, we give the definition of the feature operator F . In signal processing, a filter of convolution is usually used to extract some feature of a signal. In this paper, we also use the convolution to define F_i .

Let $\{K_i(x)\}$ be a family of functions with a compact support $E = [-r, r] \times [-r, r]$ such that $K_i(x) = 0$ for $x \in R^2 - E$ and $K_i(x) \in L^\infty(R^2, R)$. For any $f \in L^2(\Omega, R)$, we define $F_i f$ as

$$F_i f(x) = f \otimes K_i = \int_{\Omega} f(y) K_i(x - y) dy. \quad (7)$$

Since

$$\begin{aligned} \left| \int_{\Omega} f(y) K_i(x-y) dy \right|^2 &\leq \int_{\Omega} f^2(y) dy \int_{\Omega} K_i^2(x-y) dy \\ &\leq \|K_i\|_{L^\infty(R^2, R)}^2 \|f\|_{L^2(\Omega, R)}^2 \end{aligned}$$

we have $F_i f \in L^2(\Omega, R)$.

By the Fubini's theorem, we have

$$F_i^* f(x) = f \otimes \hat{K}_i = \int_{\Omega} f(y) K_i(y-x) dy, \quad (8)$$

where $\hat{K}_i(x) = K_i(-x)$.

For any $\eta = (\eta_1, \eta_2) \in C_0^1(\Omega, R^2)$, we have

$$\begin{aligned} F_i^* \operatorname{div} \eta &= \int_{\Omega} \operatorname{div} \eta(y) K_i(y-x) dy \\ &= - \int_{\Omega} \eta(y) \nabla_y (K_i(y-x)) dy \\ &= \int_{\Omega} \eta(y) \nabla_x (K_i(y-x)) dy \\ &= \int_{\Omega} \eta_1(y) \frac{\partial K_i(y-x)}{\partial x_1} + \eta_2(y) \frac{\partial K_i(y-x)}{\partial x_2} dy \\ &= \operatorname{div} \left(\int_{\Omega} \eta_1(y) K_i(y-x) dx, \int_{\Omega} \eta_2(y) K_i(y-x) dx \right) \\ &= \operatorname{div} (F_i^* \eta_1, F_i^* \eta_2) \\ &= \operatorname{div} F_i^* \eta \end{aligned}$$

where we assume $x = (x_1, x_2)$. Combining the above equation with Lemma 1, we thus have

$$F^* \operatorname{div} \eta = \operatorname{div} F^* \eta.$$

2.2 Algorithm

In this section, we utilize the split Bregman algorithm [28] to solve problem (2). Before describing the algorithm, we need to give the discrete version of Problem (2).

Let f be a matrix, such as an image of size $s \times t$, K_i a matrix convolution filter of size $(2r+1) \times (2r+1)$. Then the discrete convolution of f and K_i is defined by

$$\begin{aligned} F_i f(k, l) &= (f \otimes K_i)(k, l) = \sum_{p=k-r, q=l-r}^{p=k+r, q=l+r} f(k, l) K_i(k-p, l-q) \\ &= \sum_{p, q=-r}^r f(k-p, l-q) K_i(p, q) \end{aligned}$$

where we assume the center of K_i is the origin of coordinates and extend f circularly. By equation (8), we have

$$\begin{aligned} F_i^* f(k, l) &= (f \otimes \hat{K}_i)(k, l) = \sum_{p=k-r, q=l-r}^{p=k+r, q=l+r} f(k, l) K_i(k-p, l-q) \\ &= \sum_{p, q=-r}^r f(k-p, l-q) K_i(-p, -q) \end{aligned}$$

Let $g = (g_1, g_2, \dots, g_r)$, g_i be a matrix of size $s \times t$. Define the p-norm of g as

$$\begin{aligned} \|g\|_1 &= \sum_{i=1}^r \|g_i\|_1 \\ \|g\|_2 &= \sqrt{\sum_{i=1}^r \|g_i\|_2^2} \end{aligned}$$

Then by equation (1), the discrete version of Problem (2) is

$$\arg \min_u \left\{ E(u) = \sum_{i=1}^m \lambda_i \|\nabla F_i u\|_1 + \frac{1}{2} \|Au - f\|_2^2 \right\} \quad (9)$$

Let $d = \nabla(Fu)$, i.e. $d_i = \nabla(F_i u)$, $d^0 = b^0 = 0$, then Problem (9) is equivalent to the following iterations:

for $j=0, 1, 2$,

$$u^{j+1} = \arg \min \frac{1}{2} \|Au - f\|_2^2 + \sum_{i=1}^m \frac{\gamma_i}{2} \left\| \nabla(F_i u) - d_i^j + b_i^j \right\|_2^2 \quad (10)$$

$$d^{j+1} = \arg \min \sum_{i=1}^m \left(\lambda_i \|d_i\|_1 + \frac{\gamma_i}{2} \left\| d_i - \nabla(F_i u^{j+1}) - b_i^j \right\|_2^2 \right) \quad (11)$$

$$b_i^{j+1} = b_i^j + (\nabla(F_i u^{j+1}) - d_i^{j+1}) \quad (12)$$

The KKT condition for problem (10) is

$$A^*(Au - f) + \sum_{i=1}^m \gamma_i F_i^* \nabla^* (\nabla F_i u - d_i^j + b_i^j) = 0$$

Therefore, the solution for Problem (10) is

$$u^{j+1} = FFT^{-1} \left(\frac{FFT(\sum_{i=1}^m \gamma_i F_i^* \nabla^* (d_i^j - b_i^j) + A^* f)}{FFT(A^* A + \sum_{i=1}^m \gamma_i F_i^* \nabla^* \nabla F_i)} \right) \quad (13)$$

The solution for problem (11) can be explicitly solved:

$$d_i^{j+1} = TH(\nabla(F_i u^{j+1}) + b_i^j, \frac{\lambda_i}{\gamma_i}) \quad (14)$$

where $TH(x, T) = \text{sgn}(x) \max(|x| - T, 0)$.

At last, the algorithm is summarized in Algorithm 1.

Algorithm 1

Set the initial values $d^0 = b^0 = 0$, $k = 0$, the maximal iteration $M > 0$ and the tolerant error $tol > 0$.
while $j < M$ and $\frac{\|u^{j+1} - u^j\|}{\|u^k\|} > tol$ **do**
 Update u^{j+1} , d^{j+1} and b^{j+1} by equations (13), (14) and (12), respectively.
end while
return u^{j+1}

Remark 4. To implement Algorithm 1, if we don't consider the existence of solution, we only need F_i^* but don't need F^{-1} or F_i^{-1} .

The proof of the convergence of the split Bregman algorithm was given in [37]. The convergence of our algorithm can be proved accordingly and so is not listed here.

3 Experimental results

In this section, we conduct some numerical experiments on image denoising and image deblurring using Algorithm 1. To implement Algorithm 1, we need to construct K_i explicitly. In our experiments, the piecewise linear B-spline wavelet frame is used for constructing K_i . The filter banks of the B-spline wavelet frame are

$$\begin{aligned} [h_1(-1), h_1(0), h_1(1)] &= \frac{1}{4}[1, 2, 1] \\ [h_2(-1), h_2(0), h_2(1)] &= \frac{\sqrt{2}}{4}[1, 0, -1] \\ [h_3(-1), h_3(0), h_3(1)] &= \frac{1}{4}[-1, 2, -1]. \end{aligned}$$

Then the K_i used in our experiment are $K_1 = h_1^\dagger h_1$ and

$$K_{3(i-1)+j} = h_i^\dagger h_j, \quad i, j = 1, 2, 3. \quad (15)$$

Clearly, the feature image generated by K_1 have more even region than those by the other K_i . So in the experiments, we set a larger λ_1 and γ_1 to impose a more smooth effect on it.

By the unitary extension principle (UEP) in [38], we have that

$$F^* F = I. \quad (16)$$

Thus, $F_L^{-1} = F^*$. By Lemma 1 and (16), we also have

$$\sum_{i=1}^m F_i^* F_i = 1 \quad (17)$$

If we set the parameter vector γ as $\gamma_1 > \gamma_2 = \gamma_3 = \dots = \gamma_m$, then by equation (17), we have

$$\begin{aligned} \sum_{i=1}^m \gamma_i F_i^* \nabla^* \nabla F_i &= (\gamma_1 - \gamma_2) F_1^* F_1 \nabla^* \nabla + \gamma_2 \nabla^* \nabla \sum_{i=1}^m F_i^* F_i \\ &= (\gamma_1 - \gamma_2) F_1^* F_1 \nabla^* \nabla + \gamma_2 \nabla^* \nabla, \end{aligned}$$

where we can interchange these operators since they are all convolutions. Thus equation (13) in Algorithm 1 can be reduced to

$$u^{j+1} = FFT^{-1} \left(\frac{FFT(\sum_{i=1}^m \lambda_i F_i^* \nabla^* (d_i^j - b_i^j) + A^* f)}{FFT(A^* A + (\gamma_1 - \gamma_2) F_1^* F_1 \nabla^* \nabla + \gamma_2 \nabla^* \nabla)} \right) \quad (18)$$

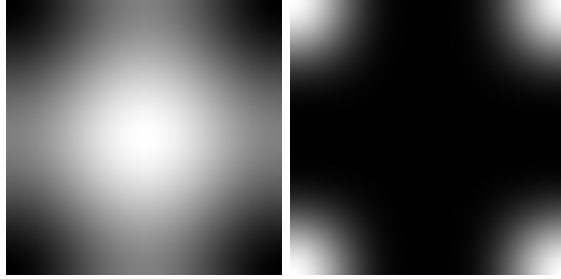


Figure 1: From left to right: FFTs of $\nabla^* \nabla$ and $F_1^* F_1$.

In Figure 1, we show the Fast Fourier transform (FFT) of $\nabla^* \nabla$ and $F_1^* F_1$, from which we can see that the effect of the FFT of $F_1^* F_1$ is opposite to that of $\nabla^* \nabla$. Since the effect of $\nabla^* \nabla$ is smoothing the image, the term $F_1^* F_1$ may slow down the convergence speed and cause artifacts in the denoised images. Thus in the numerical simulations, we neglect the term $(\gamma_1 - \gamma_2) F_1^* F_1 \nabla^* \nabla$ for computational efficiency. Equation (18) is thus changed into

$$u^{j+1} = FFT^{-1} \left(\frac{FFT(\gamma \sum_{i=1}^m \lambda_i F_i^* \nabla^* (d_i^j - b_i^j) + A^* f)}{FFT(A^* A + \gamma_1 \nabla^* \nabla)} \right) \quad (19)$$

Equation (19) can be seen as an analogy of the original split Bregman algorithm who solves u^{j+1} by

$$u^{j+1} = FFT^{-1} \left(\frac{FFT(\lambda \nabla^* (d^j - b^j) + A^* f)}{FFT(A^* A + \gamma_1 \nabla^* \nabla)} \right)$$

By experiments, we find that using equation (19) can indeed get better results than using equation (13). To demonstrate it, we give both results of using equations (13) and (19) in the compared experiments.

In Section 3.1, we compare the experimental results of our model with the related methods (such as split Bregman algorithm (SB) [28], dual tree complex wavelet transform (DTCWT) [39], local contextual hidden markov model

(LHMM) [15] and the l_o minimization in wavelet frame based model (l_o -WF) [40]. In Section 3.2, we perform the comparison on the simulation of image deblurring with our model, the l_o -WF model and the EDWF[41] model. For measuring the image quality quantitatively, we use the index peak signal to noise ratio (PSNR) defined by

$$PSNR := 10\log_{10}\left(\frac{255 * 255 * N}{\|ref - \tilde{u}\|_2^2}\right)$$

where ref and \tilde{u} are the true image and recovered image, respectively.

3.1 Image denoising

In this subsection, we compare the performances of our model with SB, DTCWT, LHMM and l_o -WF on image denoising. Six images (all of size 256*256) shown in Figure 2 are tested. The noisy images are generated by the MATLAB command ‘innoise’ with ‘type=Guassian’, $m = 0$ and variance $v = 0.01$.



Figure 2: The test images.

In the implementation of image denoising, the parameters of our algorithm using equation (13) are set as: $\lambda_1 = \lambda_2 = \dots = \lambda_9 = 0.2$, $\gamma_1 = 8$, $\gamma_2 = \gamma_3 = \dots = \gamma_9 = 4$, $tol = 1e - 4$; the parameters of our algorithm using equation (19) are set as: $\lambda_1 = 2$, $\lambda_2 = \lambda_3 = \dots = \lambda_9 = 1.5$, $\gamma_1 = 12$, $\gamma_2 = \gamma_3 = \dots = \gamma_9 = 4.5$, $tol = 5e - 4$. For SB algorithm, the parameters are set as: $\lambda = 19$, $gamma = 1$, $tol = 5e - 4$. For DTCWT, the decomposition level $L = 4$, threshold $T = 20$. For l_o -WF, the piecewise linear B-spline wavelet frame is also used and the decomposition level $L = 1$, $\lambda = 350$, $\mu = 1$, $\gamma = 0.2$, $tol = 5e - 4$. The

LHMM model has no free parameters. For fair comparison, all the parameters are uniformly set for the six tested images and we try our best to tune them to get the highest average PSNR.

In Figure 3, we show the feature (coefficient) images of a noisy image and its denoised version by our method using equation (19). From Figure 3, we can see that the noises in every feature images are all removed.

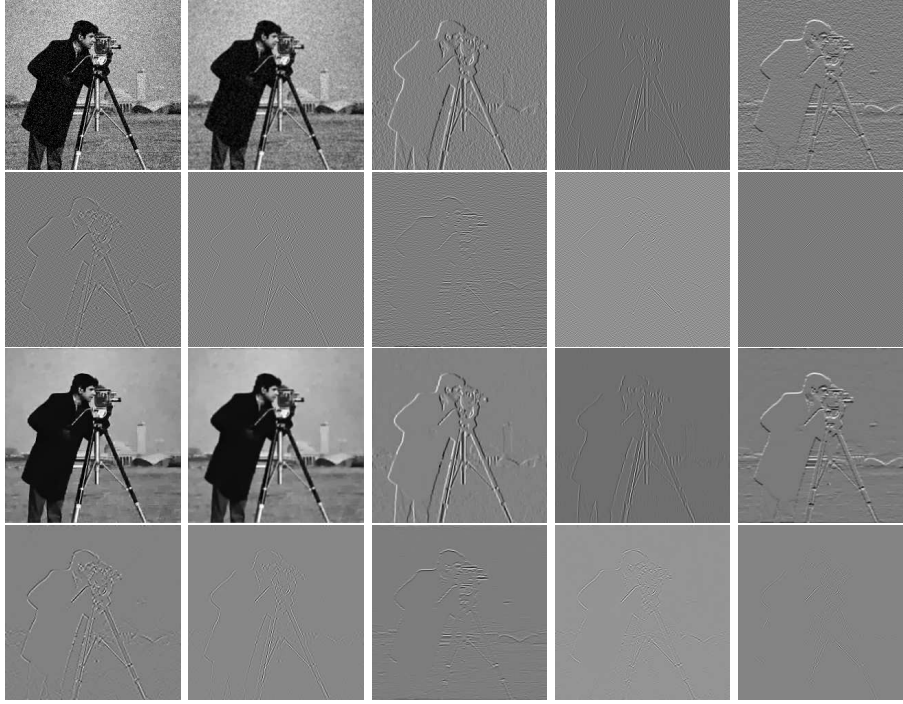


Figure 3: The feature images of the noisy and denoised.

In Figure 4 - Figure 9, we show the visual comparisons of the results from the four compared methods. From the results of SB, we can see that the recovered images have a lot of artifacts in the homogeneous regions. The reason is that the regularization parameter λ is chosen optimal for PSNR value. In order to preserve the sharp edges in images, a relatively small λ should be chosen. However, it leads to lack of smoothness in homogeneous regions. This visual effect is especially clear in the ‘cameraman’ image (see the sky and grass). From the results of DTCWT and LCHMM, we can observe that the restored images introduce too much artifacts. One of the reasons is that they both use the decimated wavelet transform. From the last three results, we can see that the denoised images by l_o -WF and ours have similar visual effects, but our method has a slightly higher PSNR and less runtime averagely which can be seen in Table 1.

Table 1 lists the PSNR and total run-time of the compared five methods

for image denoising. Since the LCHMM is coded by C++ and the others by matlab, we don't list the runtime of LCHMM. From Table 1, we can see that our model outperforms the other image restoration methods in terms of PSNR, averagely. In addition, from Table 1, we can see that the DTCWT is the fastest (It spends less than 1 second for the six test images). However, the quality of the DTCWT is the worst.

To show the convergence of the our algorithm using equation (19), we plot the relative error $\frac{\|u^{n+1}-u^n\|}{\|u^n\|}$ versus the iterations of the six test images in Figure 10. From Figure 10, we can observe the relative error is monotonically decreasing with the iterations, which numerically proves that the algorithm is convergent.



Figure 4: Comparison for image denoising. From left to right and up to down are: noisy images and denoised by SB, DTCWT, LCHMM, l_o -WF and ours using equations (13) and (19), respectively.

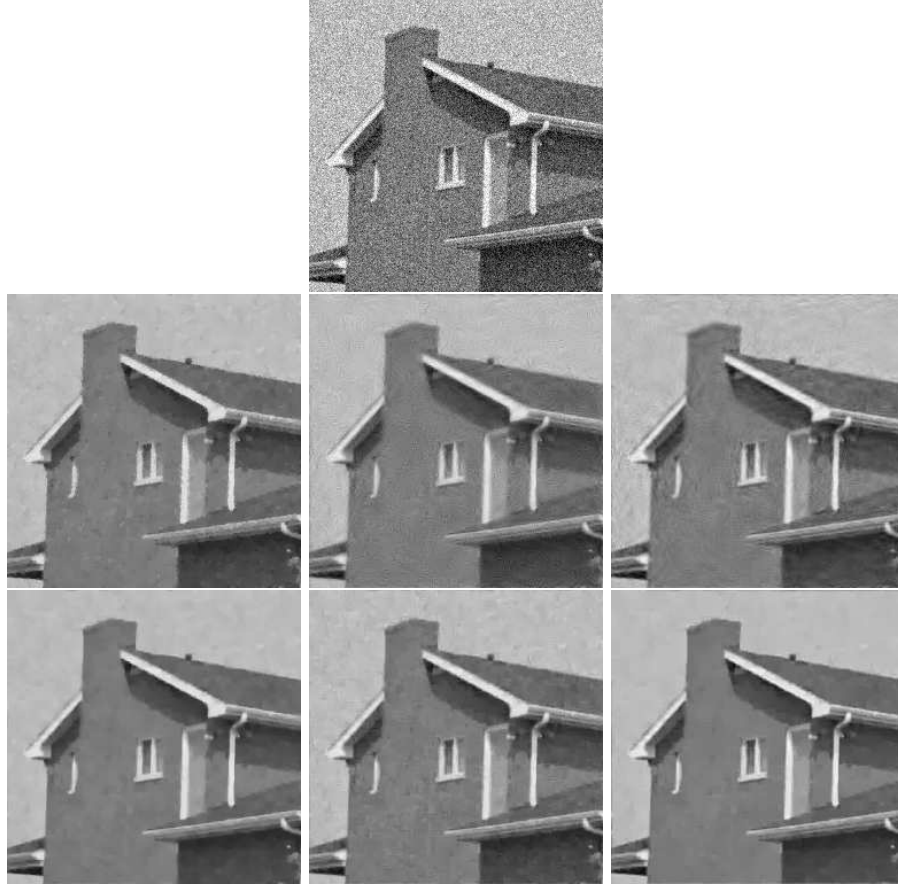


Figure 5: Comparison for image denoising. From left to right and up to down are: noisy images and denoised by SB, DTCWT, LCHMM, l_o -WF and ours using equations (13) and (19), respectively.

Table 1: PSNR of the compared four methods for image denoising

Image	original	SB	DTCWT	LCHMM	l_o -WF	ours using (13)	ours using (19)
1	20.45	27.05	26.21	27.14	27.63	27.35	27.81
2	20.04	30.20	28.45	29.78	31.17	30.63	30.99
3	20.07	25.64	25.28	26.00	25.88	26.38	26.36
4	20.15	26.16	25.78	26.47	26.40	26.66	26.69
5	20.06	27.64	27.09	27.98	27.98	28.12	28.18
6	20.17	27.89	27.17	28.08	28.20	28.23	28.33
average	20.17	27.43	26.66	27.57	27.88	27.89	28.06
Time(s)	-	3.09	0.49	-	12.40	10.00	4.02



Figure 6: Comparison for image denoising. From left to right and up to down are: noisy images and denoised by SB, DTCWT, LCHMM, l_o -WF and ours using equations (13) and (19), respectively.

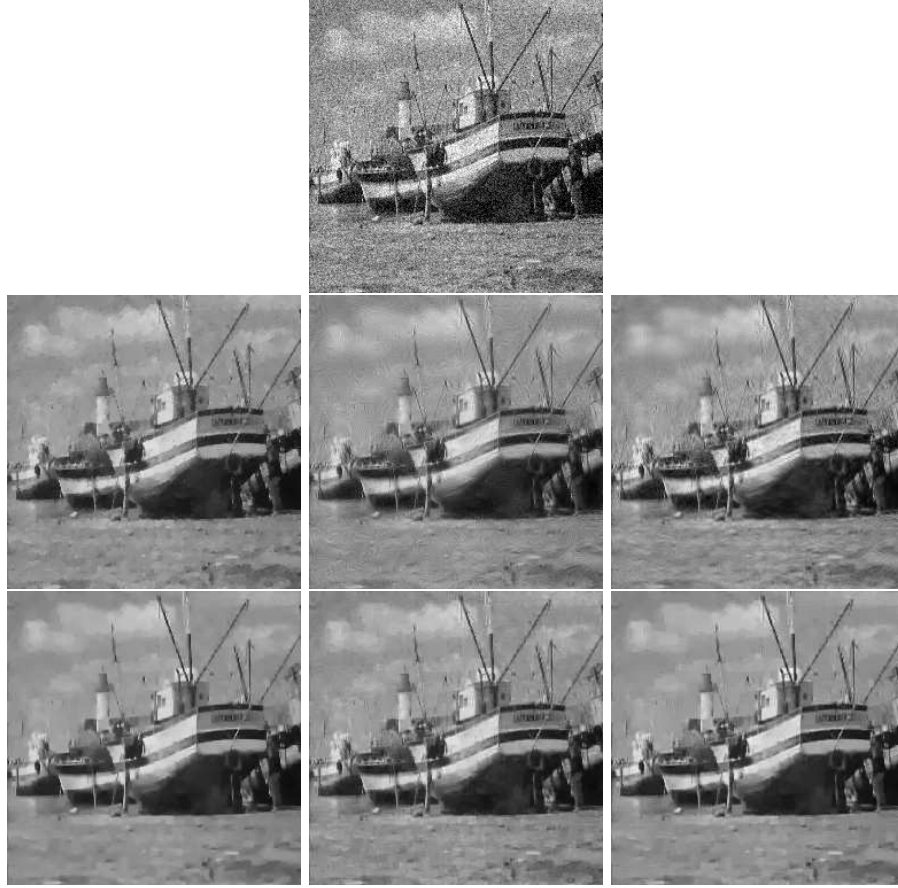


Figure 7: Comparison for image denoising. From left to right and up to down are: noisy images and denoised by SB, DTCWT, LCHMM, l_o -WF and ours using equations (13) and (19), respectively.



Figure 8: Comparison for image denoising. From left to right and up to down are: noisy images and denoised by SB, DTCWT, LCHMM, l_o -WF and ours using equations (13) and (19), respectively.



Figure 9: Comparison for image denoising. From left to right and up to down are: noisy images and denoised by SB, DTCWT, LCHMM, l_o -WF and ours using equations (13) and (19), respectively.

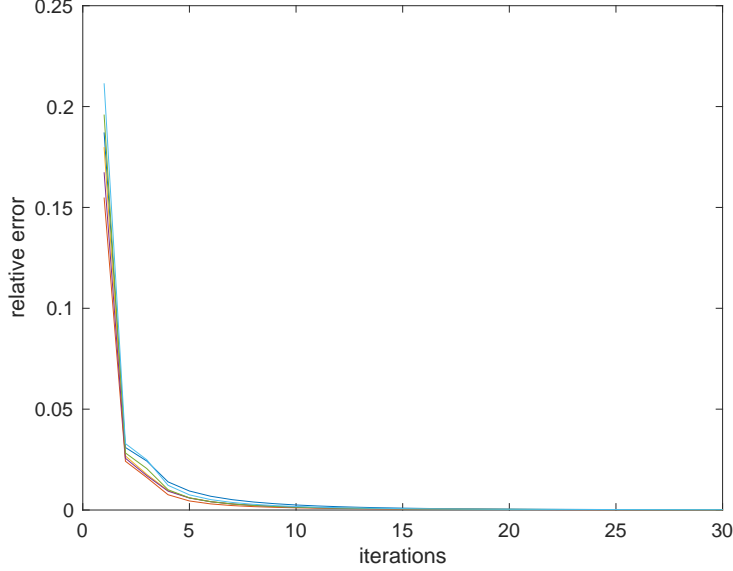


Figure 10: Relative error $\frac{\|u^{n+1}-u^n\|}{\|u^n\|}$ versus iterations of six test images.

3.2 Image deblurring

In this subsection, we apply the proposed model to image deblurring and compare the results with those of l_o -WF and EDWF. We also test the same six images for image deblurring. The blurred images are generated by convolution with the blur kernel A and added by a Gaussian noise η , where A and η are generated by the MATLAB command ' $A = fspecial('motion', 9, 0)$ ' and ' $\eta = 5 * randn(size(u))$ ', respectively.

In the implementation of image deblurring, the parameters of our model using equation (13) are set as: $\lambda_1 = 0.006$, $\lambda_2 = \dots = \lambda_9 = 0.004$, $\gamma_1 = 0.4$, $\gamma_2 = \gamma_3 = \dots = \gamma_9 = 0.1$, $tol = 5e - 4$; the parameters of our algorithm using equation (19) are set as: $\lambda_1 = 0.004$, $\lambda_2 = \lambda_3 = \dots = \lambda_9 = 0.002$, $\gamma_1 = 0.1$, $\gamma_2 = \gamma_3 = \dots = \gamma_9 = 0.4$, $tol = 5e - 4$. For l_o -WF, the piecewise linear B-spline wavelet frame is also used and the decomposition level $L = 1$, $\lambda = 30$, $\mu = 0.01$, $\gamma = 0.003$, $tol = 5e - 4$. For EDWF, $\lambda = 1$, $\gamma = 1.5$, $\rho = 0.2$, $v = 0.15$, $\mu_1 = 1$, $\mu_2 = 1$.

In Figure 11, the visual results of the three models are presented and Table 2, summarizes the PSNR and total run-time of the three methods. From Table 2, we can see that the PSNR of our model using equation (19) is averagely the largest.



Figure 11: Comparison for image deblurring. From left to right are: blurry images and deblurred by l_o -WF, EDWF and ours using equations (13) and (19), respectively.

Table 2: PSNR of the compared four methods for image deblurring

Image	original	l_o -WF	EDWF	ours using (13)	ours using (19)
1	21.43	26.25	26.16	26.72	26.85
2	26.50	32.55	31.77	32.56	32.61
3	22.75	25.60	25.44	25.94	25.98
4	22.57	25.39	25.31	25.78	25.82
5	24.28	28.07	27.70	28.14	28.17
6	22.63	27.73	27.56	27.94	28.02
average	23.36	27.60	27.32	27.84	27.91
Total Time(s)	-	26.67	141.34	7.67	7.76

4 Conclusions

In this paper, we proposed a vector total variation (VTV) of feature image model for image restoration. The VTV imposes different smoothing powers on different features and thus can simultaneously preserve edges and remove noises. Next, the existence of solution for the model was proved and the split Bregman algorithm was used to solve the model. At last, we used the wavelet filter banks to explicitly define the feature operator and presented some experimental results to show its advantage over the related methods in both quality and efficiency.

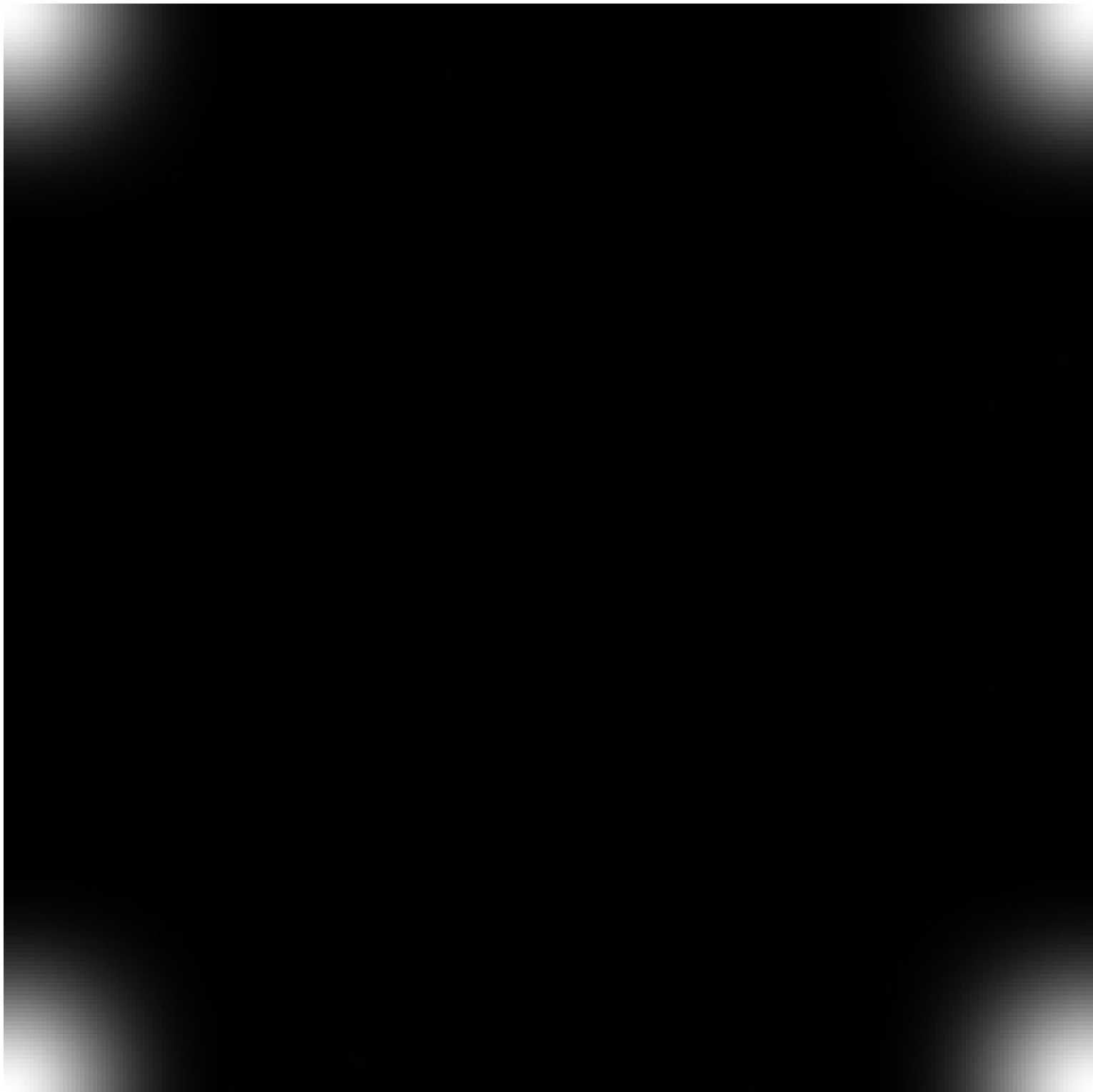
References

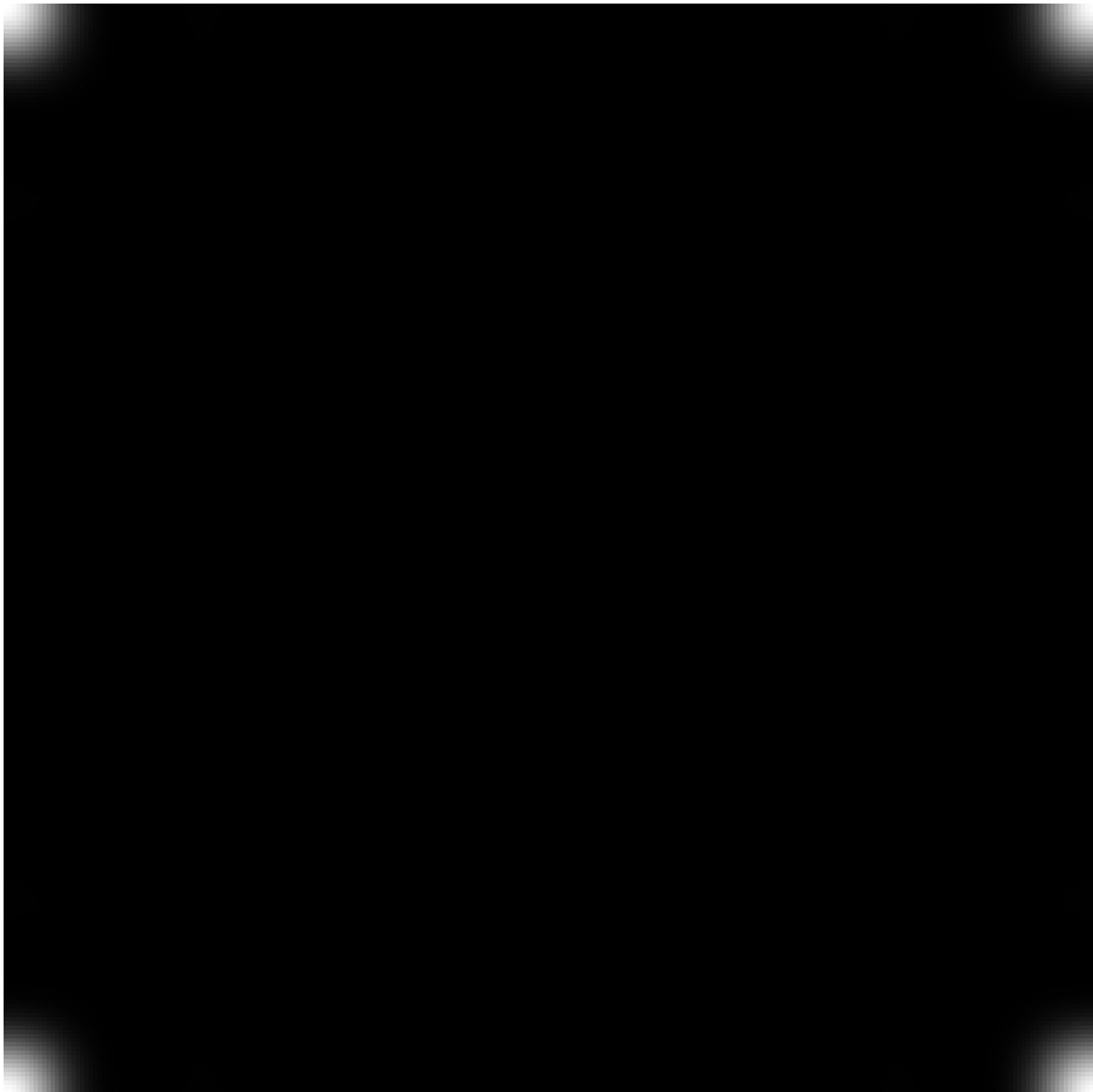
- [1] R. Choksi, Y. Van Gennip, and A. Oberman. Anisotropic total variation regularized l^1 -approximation and denoising/deblurring of 2D bar codes. *Inverse Problems & Imaging*, 5(3):591–617, 2017.
- [2] A. Marquina. Nonlinear inverse scale space methods for total variation blind deconvolution. *SIAM Journal on Imaging Sciences*, 2(1):64–83, 2009.
- [3] T. F. Chan and C. K. Wong. Total variation blind deconvolution. *IEEE Transactions on Image Processing*, 7(3):370–375, 1998.
- [4] Y. W. Wen, R. H. Chan, and A. M. Yip. A primal-dual method for total-variation-based wavelet domain inpainting. *IEEE Transactions on Image Processing*, 21(1):106–114, 2012.
- [5] M. Ng, F. Wang, and X. M. Yuan. Fast minimization methods for solving constrained total-variation superresolution image reconstruction. *Multidimensional Systems and Signal Processing*, 22(1):259–286, 2011.
- [6] K. Bredies and M. Holler. A total variation-based JPEG decompression model. *SIAM Journal on Imaging Sciences*, 5(1):366–393, 2012.

- [7] W. Wang and C. He. A variational model with barrier functionals for Retinex. *SIAM Journal on Imaging Sciences*, 8(3):1955–1980, 2015.
- [8] J. F. Cai, S. Osher, and Z. Shen. Linearized bregman iterations for frame-based image deblurring. *SIAM Journal on Imaging Sciences*, 2(1):226–252, 2009.
- [9] C. Chaux, P. L. Combettes, J. C. Pesquet, and V. R. Wajs. A variational formulation for frame-based inverse problems. *Inverse Problems*, 23(4):1495, 2011.
- [10] M. J. Fadili, J. L. Starck, and F. Murtagh. Inpainting and zooming using sparse representations. *Computer Journal*, 52(1):64–79, 2009.
- [11] M. A. Figueiredo and R. D. Nowak. An EM algorithm for wavelet-based image restoration. *IEEE Transactions on Image Processing*, 12(8):906–16, 2003.
- [12] J. F. Cai, S. Osher, and Z. Shen. Split bregman methods and frame based image restoration. *SIAM Journal on Multiscale Modeling & Simulation*, 8(2):337–369, 2009.
- [13] M. Elad, J. L. Starck, P. Querre, and D. L. Donoho. Simultaneous cartoon and texture image inpainting using morphological component analysis (MCA). *Applied & Computational Harmonic Analysis*, 19(3):340–358, 2005.
- [14] J. L. Starck, M. Elad, and D. L. Donoho. Image decomposition via the combination of sparse representations and a variational approach. *IEEE Transactions on Image Processing*, 14(10):1570–82, 2005.
- [15] G. Fan and X.-G. Xia. Image denoising using a local contextual hidden markov model in the wavelet domain. *IEEE Signal Processing Letters*, 8(5):125–128, 2001.
- [16] J. F. Cai, R. Chan, L. Shen, and Z. Shen. Restoration of chopped and nodded images by framelets. *SIAM Journal on Scientific Computing*, 30(3):1205–1227, 2007.
- [17] J. F. Cai, R. H. Chan, and Z. Shen. A framelet-based image inpainting algorithm. *Applied & Computational Harmonic Analysis*, 24(2):131–149, 2008.
- [18] R. H. Chan, S. D. Riemenschneider, L. Shen, and Z. Shen. Tight frame: an efficient way for high-resolution image reconstruction. *Applied & Computational Harmonic Analysis*, 17(1):91–115, 2004.
- [19] L. I. Rudin, S. Osher, and E. Fatemi. Nonlinear total variation based noise removal algorithms. *Physica D Nonlinear Phenomena*, 60(14):259–268, 1992.

- [20] G. Gilboa and S. Osher. Nonlocal operators with applications to image processing. *SIAM Journal on Multiscale Modeling & Simulation*, 7(3):1005–1028, 2008.
- [21] S. M. Chao and D. M. Tsai. An improved anisotropic diffusion model for detail- and edge-preserving smoothing. *Pattern Recognition Letters*, 31(13):2012–2023, 2010.
- [22] C. Louchet and L. Moisan. Total variation as a local filter. *SIAM Journal on Imaging Sciences*, 4(2):651–694, 2014.
- [23] C. Sutour, C. A. Deledalle, and J. F. Aujol. Adaptive regularization of the nl-means: application to image and video denoising. *IEEE Transactions on Image Processing*, 23(8):3506–3521, 2014.
- [24] A. Chambolle. An algorithm for total variation minimization and applications. *Journal of Mathematical Imaging and Vision*, 20:89–97, 2004.
- [25] M. Zhu and T. F. Chan. An efficient primal-dual hybrid gradient algorithm for total variation image restoration. *UCLA Cam. Report*, 2008.
- [26] A. Beck and M. Teboulle. Fast gradient-based algorithms for constrained total variation image denoising and deblurring problems. *IEEE Transactions on Image Processing*, 18(11):2419, 2009.
- [27] E. Esser, X. Zhang, and T. F. Chan. A general framework for a class of first order primal-dual algorithms for convex optimization in imaging science. *SIAM Journal on Imaging Sciences*, 3(4):1015–1046, 2010.
- [28] T. Goldstein and S. Osher. The split bregman method for L1-Regularized problems. *SIAM Journal on Imaging Sciences*, 2(2):323–343, 2009.
- [29] A. Chambolle and T. Pock. A first-order primal-dual algorithm for convex problems with applications to imaging. *Journal of Mathematical Imaging and Vision*, 40(1):120–145, 2011.
- [30] W. Wang and C. He. A fast and effective algorithm for a poisson denoising model with total variation. *IEEE Signal Processing Letters*, 24(3):269–273, 2017.
- [31] V. Duval, J. F. Aujol, and L. Vese. A projected gradient algorithm for color image decomposition. *Journal of Mathematical Imaging & Vision*, 2008.
- [32] B. Goldluecke and D. Cremers. An approach to vectorial total variation based on geometric measure theory. In *2010 IEEE Computer Society Conference on Computer Vision and Pattern Recognition*, pages 327–333, June 2010.
- [33] L. Ambrosio, N. Fusco, and D. Pallara. *Functions of Bounded Variation and Free Discontinuity Problems*. Oxford mathematical monographs, Oxford University Press,, 2000.

- [34] G. Aubert and P. Kornprobst. *Mathematical Problems in Image Processing: Partial Differential Equations and the Calculus of Variations*, volume 147. Springer Verlag, Applied Mathematical Sciences, 2001.
- [35] X. Bresson and T. F. Chan. Fast dual minimization of the vectorial total variation norm and applications to color image processing. *Inverse Problems & Imaging*, 2(4):455–484, 2017.
- [36] L. Vese. A study in the BV space of a denoising-deblurring variational problem. *Applied Mathematics and Optimization*, 44(2):131–161, 2001.
- [37] J. Cai, S. Osher, and Z. Shen. Split bregman methods and frame based image restoration. *Multiscale Modeling & Simulation*, 8(2):337–369, 2010.
- [38] A. Ron and Z. Shen. Affine systems in $l_2(r^d)$: The analysis of the analysis operator*. *Journal of Functional Analysis*, 148(2):408–447, 1997.
- [39] I. W. Selesnick, R. G. Baraniuk, and N. C. Kingsbury. The dual-tree complex wavelet transform. *IEEE Signal Processing Magazine*, 22(6):123–151, 2005.
- [40] B. Dong and Y. Zhang. An efficient algorithm for l_0 minimization in wavelet frame based image restoration. *Journal of Scientific Computing*, 54(2-3):350–368, 2013.
- [41] J. K. Choi, B. Dong, and X. Zhang. An edge driven wavelet frame model for image restoration. *arXiv:1701.07158*, 2017.





-
- A solid black rectangle.

the 1990s, the number of people in the UK who are aged 65 and over has increased by 1.5 million, and the number of people aged 75 and over has increased by 1.2 million (Office of National Statistics 1999). The number of people aged 65 and over is projected to increase to 6.5 million by 2011, and the number of people aged 75 and over to 4.5 million (Office of National Statistics 1999).

There is a growing awareness of the need to develop services to meet the needs of older people, and a number of initiatives have been developed to address this need. The Department of Health (1999) has published a strategy for older people, which sets out the government's commitment to improve the lives of older people. The strategy is based on three main principles: (1) to ensure that older people have the opportunity to live independently and actively; (2) to ensure that older people have access to the services and support they need; and (3) to ensure that older people are treated with respect and dignity.

The strategy is based on three main principles: (1) to ensure that older people have the opportunity to live independently and actively; (2) to ensure that older people have access to the services and support they need; and (3) to ensure that older people are treated with respect and dignity. The strategy is based on three main principles: (1) to ensure that older people have the opportunity to live independently and actively; (2) to ensure that older people have access to the services and support they need; and (3) to ensure that older people are treated with respect and dignity.

The strategy is based on three main principles: (1) to ensure that older people have the opportunity to live independently and actively; (2) to ensure that older people have access to the services and support they need; and (3) to ensure that older people are treated with respect and dignity. The strategy is based on three main principles: (1) to ensure that older people have the opportunity to live independently and actively; (2) to ensure that older people have access to the services and support they need; and (3) to ensure that older people are treated with respect and dignity.

The strategy is based on three main principles: (1) to ensure that older people have the opportunity to live independently and actively; (2) to ensure that older people have access to the services and support they need; and (3) to ensure that older people are treated with respect and dignity. The strategy is based on three main principles: (1) to ensure that older people have the opportunity to live independently and actively; (2) to ensure that older people have access to the services and support they need; and (3) to ensure that older people are treated with respect and dignity.

The strategy is based on three main principles: (1) to ensure that older people have the opportunity to live independently and actively; (2) to ensure that older people have access to the services and support they need; and (3) to ensure that older people are treated with respect and dignity. The strategy is based on three main principles: (1) to ensure that older people have the opportunity to live independently and actively; (2) to ensure that older people have access to the services and support they need; and (3) to ensure that older people are treated with respect and dignity.

The strategy is based on three main principles: (1) to ensure that older people have the opportunity to live independently and actively; (2) to ensure that older people have access to the services and support they need; and (3) to ensure that older people are treated with respect and dignity. The strategy is based on three main principles: (1) to ensure that older people have the opportunity to live independently and actively; (2) to ensure that older people have access to the services and support they need; and (3) to ensure that older people are treated with respect and dignity.

The strategy is based on three main principles: (1) to ensure that older people have the opportunity to live independently and actively; (2) to ensure that older people have access to the services and support they need; and (3) to ensure that older people are treated with respect and dignity. The strategy is based on three main principles: (1) to ensure that older people have the opportunity to live independently and actively; (2) to ensure that older people have access to the services and support they need; and (3) to ensure that older people are treated with respect and dignity.

The strategy is based on three main principles: (1) to ensure that older people have the opportunity to live independently and actively; (2) to ensure that older people have access to the services and support they need; and (3) to ensure that older people are treated with respect and dignity. The strategy is based on three main principles: (1) to ensure that older people have the opportunity to live independently and actively; (2) to ensure that older people have access to the services and support they need; and (3) to ensure that older people are treated with respect and dignity.